2024 IEEE International Conference on Robotics and Automation (ICRA 2024)
May 13-17, 2024. Yokohama, Japan

A Novel Robotic Bronchoscope with a Spring-Based Extensible Segment for Improving Steering Ability

Jie Wang, Chengquan Hu, Jingyi Kang, Jiayuan Liu, Longfei Ma and Hongen Liao*

Abstract— **Bronchoscopy, as an essential minimally invasive diagnostic and therapeutic modality, assumes a pivotal role in the early detection of lung cancer. However, the complex anatomy of the airway and the fixed length of the bronchoscope's bending segment, along with its external propulsion property, pose challenges, including the risk of bleeding. This paper introduces a 4 mm diameter robot-assisted bronchoscope with a spring-based extensible segment. By manipulating two driven rods, the segment can be lengthened or shortened. The advantages of the extensible segment are discussed in two main aspects through theoretical analysis and experimentation. Firstly, the extensible segment enables the bronchoscope to move in a follow-the-leader motion mode or fixed-angle motion mode, navigating through narrow corners that are inaccessible to fixed-length bronchoscopes. It can also be shortened to increase its stiffness when it reaches the target position, creating a stable surgical platform for procedures like biopsies. In addition, a tailored master device has been developed to control the extensible bronchoscope in an isotropic manner. Phantom experiments confirm the feasibility and effectiveness of the extensible bronchoscope.**

I. Introduction

Lung cancer remains one of the primary causes of death worldwide due to the challenge of early detection [1]. In addition to the technique of transthoracic needle aspiration biopsy [2], bronchoscopy - which includes both rigid bronchoscopy [3] and flexible bronchoscopy [4] - serves as an essential tool for diagnosing and staging the disease through biopsies. To safely and effectively sample pulmonary lesions, a range of advanced bronchoscopy technologies have been developed, including virtual bronchoscopy [5], radial endobronchial ultrasound [6], and electromagnetic navigation [7]. Robotic assisted bronchoscopy (RAB) is further developed to increase diagnostic yield, such as the two leading robotic bronchoscopy platforms, Monarch^{TM} platform by Auris Health Inc. and Ion^{TM} Endoluminal System by Intuitive Surgical [8], [9].

To address the challenge of early diagnosis utilizing current bronchoscopes, two technological aspects are vital: navigation and an advanced robotic platform. The former encompasses airway medical image segmentation, 3D model reconstruction, and robot positioning as well as shape and force sensing. The latter is concerned with the dimension and steering capabilities of bronchoscopes. The steering ability means that the bronchoscopes' distal tip can steer towards the desired peripheral lung bronchus under the external propulsion property. Navigating complex airways geometrically depends on three key parameters: the length of the distal bending section, and the bronchoscope's diameter and bending angle. The diameter factor will not be discussed in this paper. The literature [10] reports a maximum bifurcation angle of about 90° between branches, which is easily accommodated with the current RAB. This paper aims to enhance the bronchoscope's manoeuvrability by actively adjusting the bending length.

In theory, bronchoscopes with shorter steering segments are optimal for confined spaces, whereas bronchoscopes with longer steering segments are more suitable for wider spaces with identical bending curvature. Therefore, if bronchoscopes were designed with a variable bending length (VBL) section, their steering ability would be significantly enhanced.

To achieve the VBL feature, three approaches are available. The first option is the concentric tube robot (CTR) [11], [12], which comprises of nested tubes. The VBL feature is located within the inner tube that protrudes from the outer tube. It can be easily controlled by rotating and extending each tube from the proximal end. However, the application of CTRs in bronchoscopes is hindered by their limited bending curvature [13]–[15]. The second approaches is continuum robots with constrained tubes [13], [16] or shafts [17]–[19]. As such, the bending length of the continuum robots will demonstrate the VBL ability as long as the constrained tubes or shafts move along the continuum robots coaxially. However, this technique adds an additional restricted tube or shaft, which obstructs the miniaturisation of the bronchoscope and diminishes flexibility in the proximal segment. The third VBL method can be seen in continuum robots with extensible segments (ES), typically intended for follow-the-leader (FTL) motion control [20]. Amanov et al. [21] proposed a tendon-driven continuum robot with an extendable section that can be controlled by push/pull actions on the backbone. Spacer discs equipped with magnets help maintain the uniformity of the bending section. However, the design presents a challenging miniaturisation problem as the central channel of the manipulator is already occupied, making it unsuitable for improving the steering ability of bronchoscopes [22]. Other methods, such as the interlaced continuum robot [23] and the MemoSlide (a complex mechanical actuator) [24], [25], also face spatial restrictions.

To enhance bronchoscope steering, this paper presents a novel robotic bronchoscope with a spring-based ES. To the

This work is supported in part by the National Natural Science Foundation of China under Grant 82027807, Grant 62201315, and Grant 81901844, and in part by Beijing Municipal Natural Science Foundation under Grant 7212202 and Grant L192013.

Jie Wang, Chengquan Hu, Jingyi Kang, Jiayuan Liu, Longfei Ma and Hongen Liao are with the Department of Biomedical Engineering, School of Medicine, Tsinghua University, Beijing 100084, China.

Corresponding author: Hongen Liao, liao@tsinghua.edu.cn.

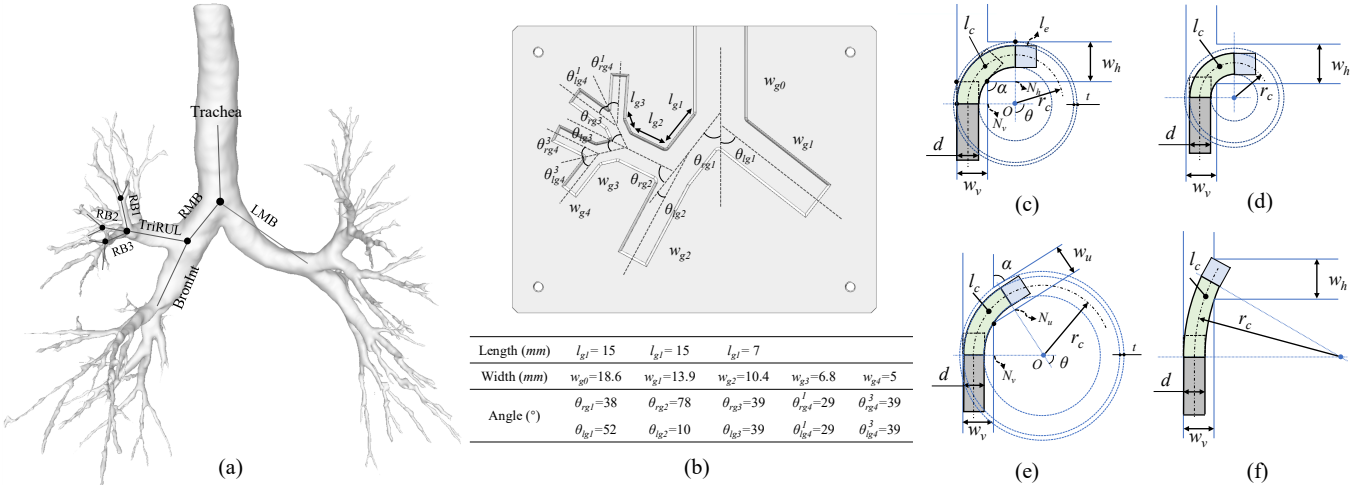

Length (*mm*)	l_{g1}= 15	l_{g1}= 15	l_{g1}= 7		
Width (*mm*)	w_{g0}=18.6	w_{g1}=13.9	w_{g2}=10.4	w_{g3}=6.8	w_{g4}=5
Angle (°)	θ_{rg1}=38	θ_{rg2}=78	θ_{rg3}=39	θ^1_{rg4}=29	θ^3_{rg4}=39
	θ_{lg1}=52	θ_{lg2}=10	θ_{lg3}=39	θ^1_{lg4}=29	θ^3_{lg4}=39

Fig. 1. Problem statement of the proposed bronchoscope with an ES. (**a**) presents a model of the human airway (RMB: right main bronchus, LMB: left main bronchus, TriRUL: right upper lobe trifurcation, BronInt:bronchus intermedius, RB$i(i = 1, 2, 3)$: i-th right bronchus). (**b**) displays the designed airway phantom with detailed dimensions. Bending manipulators, consisting of three parts: the proximal rigid shaft (grey area), the bending segment (green area), and the distal end shaft (blue area), with varying lengths are shown to compare their steering ability: just right pass thorough the right-angle bend (**c**) and the acute-angle bend (**e**), pass through the right-angle bend more easily with a shorter bending segment (**d**) than with a longer bending segment (**f**).

best of our knowledge, this is the first attempt to utilize the VBL feature with an ES to enhance the steering capability of the bronchoscope. The spring-based ES is improved based on our previous work [26] by replacing the driven cable with the Ni-Ti rod. The elongation and shortening of the designed extensible robotic bronchoscope (ERB) is controlled by simultaneously pushing and pulling the two driven Ni-Ti rods. The paper presents a clear distinction from our previous work [27], which is reflected in the following aspects:

1) The work [27] focuses on the performance validation of an extensible manipulator, while this paper proposes a novel robotic bronchoscope with a spring-based extensible segment.
2) The proposed ERB, coupled with the VBL feature, has the potential to decrease the risk of bronchial wall haemorrhage by reducing the need for repeated insertions as a result of steering issues.
3) The ERB's ES can increase its bending stiffness if the bending length is reduced. This is essential for creating a reliable platform for lesion sampling when the bronchoscope reaches its target.

In summary, this paper presents the following contributions:

1) A robotic bronchoscope with an ES to improve steering ability is proposed, fabricated and validated for the first time in this paper.
2) An adapted actuator for the ERB with a constrained mechanism is proposed, taking into account the compression situation of the driven rod.
3) A tailored master device is developed to operate the ERB in an isotropic manner.

The remaining sections are structured as follows. Section II presents the advantages of the proposed ERB compared to the traditional bronchoscopes. The system design and motion control of the ERB are described in Sections III and IV, respectively. Validating experiments of the ERB are presented in Section V, followed by a conclusion in Section VII.

II. Problem Statement

The steering of the bronchoscope is impacted not just by dimensional factors but also by the method of movement (whether it follows the leader or not) while moving through a bronchial bifurcation. The ES can alter its bending length while moving in the FTL mode, providing the ERB with greater steering capability in comparison to the traditional bronchoscope. This section will examine the impact of extensible segments on the steering capability of the bronchoscope.

A three-dimensional representation of a human airway is shown in Fig. 1(**a**), created using 3D Slicer software based on data retrieved from [28]. The right upper lobe is the focus of this research paper due to its high incidence of lung cancer [29] and the complicated sampling process caused by its acute airway turns [30]. Building upon [31], we designed an airway phantom [see Fig. 1(**b**)] with detailed data from [10], [32]. This phantom will be used for subsequent experiments aiming to verify the superior steering capability of the proposed ERB.

Based on the airway model [see Fig. 1(**a**)] and the statistical data from [10], the bronchial bifurcation angles of airway are essentially acute, at most right angles. As shown in Fig. 1(**e**), an ES (refer to Fig. 3 for the design detail) steers through an acute angle α. Here, we assume that the bronchoscope can pass through the bifurcation angle smoothly and safely when the tangent angle at the anterior and posterior endpoints of the bending segment is equal to the bifurcation angle. Referring to Fig. 1(**e**), we can write

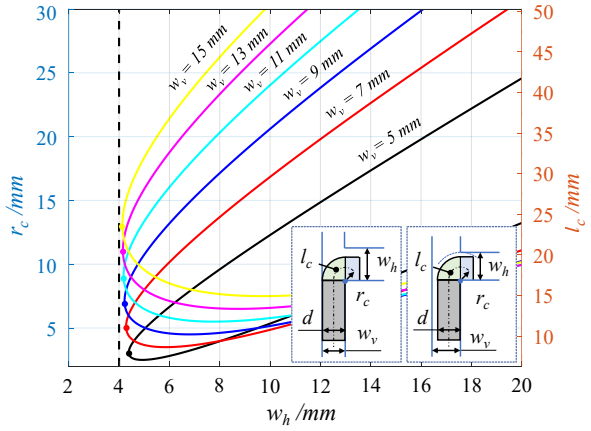

Fig. 2. Parameters of the steering segment (r_c, l_c) versus the dimensions of the right-angle bend (w_h, w_v). The insets show the cases $d = w_v$ and $d = w_h - t$. Here, α = 90°, d = 4 mm, and l_e = 2 mm.

the following equations,

$$
\begin{aligned}
&w_u - d - t + \left\|\overline{ON_u}\right\| = w_v - d + \left\|\overline{ON_v}\right\| = r_c - \frac{d}{2} \\
&arcsin(\frac{\left\|\overline{ON_u}\right\|}{r_c - \frac{d}{2}}) + arcsin(\frac{\left\|\overline{ON_v}\right\|}{r_c - \frac{d}{2}}) = \pi - \theta = \pi - \alpha \\
&(r_c + \frac{d}{2})^2 + l_e^2 = (r_c + \frac{d}{2} + t)^2 \\
&l_c = (r_c(w_u, w_v, \alpha, d, h) + \frac{d}{2})\theta.
\end{aligned} \tag{1}
$$

Where d represents the diameter of the ES, l_e stands for the length of the end rigid block, and t refers to the thickness of the increased motion space arising from the presence of the rigid end block [refer to Fig. 1(**e**)], θ denotes the bending angle, and r_c and l_c indicate the maximum bending radius and length, respectively, when the extensible manipulator crosses the bifurcation angle.

If the bifurcation angle is a right angle, i.e. $\alpha = \pi/2$, Fig. 1(**e**) will then be substituted by Fig. 1(**c**). To demonstrate the correlation between the steering manipulator (r_c, l_c) and the right-angle bend (w_h, w_v), Fig. 2 is presented based on (1). Note that there are two values (r_c, l_c) in relation to w_h, except at the leftmost point (indicated by solid dots in Fig. 2). The larger value holds significance. Fig. 2 leads to two conclusions: 1) If the bifurcation angle α remains constant, the smaller the values of w_h and w_v become, the smaller r_c and l_c should be; 2) As the length of the rigid end block increases, the bending segment's steering ability diminishes. This effect is more pronounced when the required bending length l_c is smaller, as illustrated in Fig. 2 with varying distances between the parabolic curves and the line w_h = 4 mm.

The ERB's steering ability is improved primarily in two ways. Firstly, a shorter bending length results in better steering ability (see Fig. 1(**c**) and Fig. 1(**d**)). It is evident that the bending segment depicted in Fig. 1(**d**) can be achieved through a smaller w_h. Additionally, the bending segment that

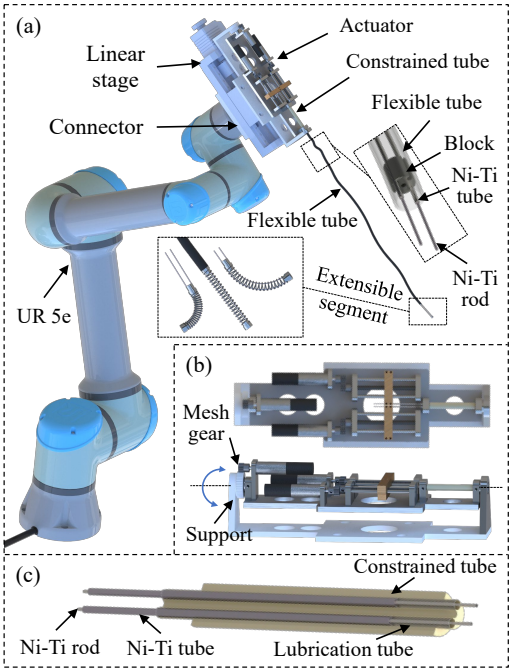

Fig. 3. Three-dimensional rendering of the proposed extensible bronchoscope.

operates in FTL mode exhibits superior steering capabilities, as evidenced by Fig. 1(**c**) and Fig. 1(**f**). It is clear that the bending segment in Fig. 1(**c**) can pass through the bends, but the bending segment shown in Fig. 1(**f**) is obstructed and unable to pass through the bend.

III. System Design

The proposed robotic bronchoscope, as illustrated in Fig. 3, features a spring-based ES. The system comprises an ES, a flexible tube, an actuator, a connector, and a UR5e (Universal Robots, Inc.) robotic arm. The connector [see Fig. 3(**a**)] attaches the actuator to the UR5e for positioning and orienting the ERB. During bronchoscopy procedures, the UR5e robot is responsible for long-distance movements, while the linear stage handles small linear movements. Thus, phantom experiments in section V-C do not include the robotic arm.

Compared to our previous research [27], this study presents three significant improvements. The first is the incorporation of a thin and long flexible tube, which is a commercially available product with the structure described in [33]. To prevent transmission errors of the Ni-Ti rod (diameter: 0.5 mm, Suzhou Xinghai e-commerce Co., LTD) within the flexible tube, a bowden control system has been designed. At the two ends of the flexible tube, two cylindrical blocks [shown in Fig. 3(**a**)] are glued, holes in which are fixed with Ni-Ti tubes (outer diameter×inner diameter: 0.9 $mm \times 0.7$ mm, Suzhou Xinghai e-commerce Co., LTD). The Ni-Ti rod travels through the Ni-Ti tube, transmitting movement and force. In addition, the actuator shown in Fig. 3(**b**) now includes an additional degree of rotation freedom. A DC motor is used to rotate the bronchoscope via

a mesh gear, with a gear manufactured in the support. Finally, to decrease the friction between the Ni-Ti rods and the constrained tube, lubricating PTFE tubes are fitted into the inner cavities of the constrained tube, as shown in Fig. 3(**c**). For additional design specifications, please refer to our earlier research [27].

IV. Motion Control

A. Workspace Analysis

This section focuses on the workspace of the proposed ES within the context of airway steering applications. While bronchoscopes are clinically controlled in a master-slave control mode, the kinematics are also significant for performance validation and future autonomous surgery [34]. Refer to our previous research [26] and [27] for details on the forward and inverse kinematics of the ES.

According to forward kinematics, the ES's workspace can be represented as shown in Fig. 4(**a**), where the proximal end of the segment is immobilised. Several particular boundary configurations are labelled in Fig. 4(**a**).

1) Configuration A represents the maximum safe travel distance of the spring. The spring's free length is not indicated in Fig. 4(**a**). For compression springs, the maximum length L_{ml} can be determined [35],

$$\begin{aligned} \tau &= \frac{16FR(4c-1)}{\pi(d_w)^3(4c-4)} < u[\tau] \\ L_{ml} &\leq \delta = \frac{F}{k}. \end{aligned} \tag{2}$$

Where the notations are defined as follows: F: the pushing force exerted by the two driven rods, R: coil radius, d_w: wire diameter, c: the spring index $c = D/d_w$, D: mean coil diameter, τ: shear stress, k: spring rate, $[\tau]$: permissible shear stress that can be obtained by a lookup table method, u: safety coefficient, δ: spring travel distance. Then the L_{ml} is the maximum value of δ.

2) Configuration E represents the minimum safe travel distance (solid height) of the spring. The minimum length of the spring, denoted L_{sl}, can be determined by $L_{sl} = nd_w$, where n stands for the number of active spring coils.

3) Configuration D and (F, a symmetry point) is a limited configuration where the spring coils come into contact. Here, we have,

$$\begin{aligned} l_r &= L_{sl} = nd_w = \pi r_r \\ l_l &= \pi(r_r + d_r) \end{aligned} \tag{3}$$

Where, d_r is the distance between the centerlines of the two driven Ni-Ti rods. r_r is defined in Fig. 4(**c**) and Fig. 5(**a**). l_r and l_l denote arc length of the corresponding radius. Accordingly, if the centerline length of the segment $L_{sl} \leq l_c \leq \pi(L_{sl}/\pi + d_r/2)$, the segment's tip will move along the arc $\overset{\frown}{DEF}$.

The kinematics yield calculations for configurations B, C, and G. As the bifurcation angle of the airway is under $90°$, the segment's bending angle in Fig. 4(**a**) is limited to $180°$.

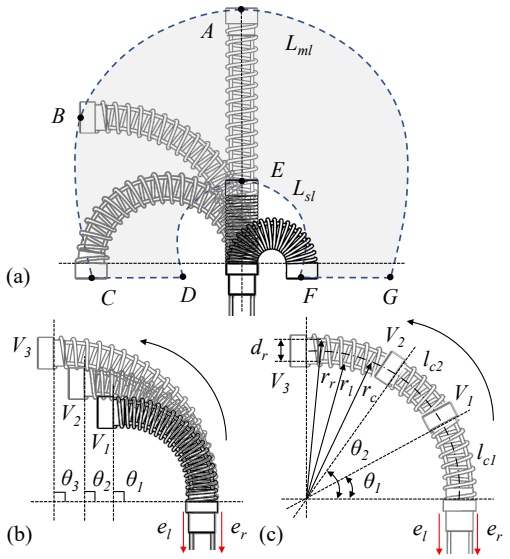

Fig. 4. Workspace analysis (**a**), fixed-angle motion mode (**b**), and fixed-radius motion mode i.e. follow-the-leader motion mode analysis (**c**) of the proposed extensible steering segment.

B. Motion Strategy

The ES is developed inspired by our previous research [26], characterised by its offset neutral bending plane. The relationship between the extension of the driven Ni-Ti rods (e_l, e_r) and the bending angle θ of the ES is as follows:

$$\theta = \frac{e_l - e_r}{d_r} = \begin{cases} > 0, & \text{segment bends to the left} \\ < 0, & \text{segment bends to the right.} \end{cases} \tag{4}$$

From (4), the bending angle θ stays constant when the discrepancy in elongation between the two driven Ni-Ti rods is fixed, i.e. $e_l - e_r = constant$, suggesting that both rods move the same distance. As shown in Fig. 4(**b**), this motion style is referred to as fixed-angle motion mode.

Fixed-radius motion mode, also known as follow-the-leader, is a crucial motion mode [20] that can decrease the occupied space during manipulator movements and enhance safety. FTL is equally significant for the ERB in this work. As shown in Fig. 4(**c**), the ES extends from configuration V_1 to V_2 to V_3. Throughout this process, the radius r_c remains constant, highlighting its FTL properties. Thus, we have,

$$\left.\begin{aligned} l_{c1} &= r_c\theta_1 \\ l_{c2} &= r_c\theta_2 \end{aligned}\right\} \Rightarrow \begin{cases} e_l' = (r_c - \dfrac{d_r}{2})(\theta_2 - \theta_1) \\ e_r' = (r_c + \dfrac{d_r}{2})(\theta_2 - \theta_1). \end{cases} \tag{5}$$

Where e_l' and e_r' indicate the length change of the two driven Ni-Ti rods when the segment transitions from the configuration V_1 to V_2.

C. Stiffness Analysis

For bronchoscopes, both flexibility and stiffness are essential features. Flexibility ensures safe interaction between the bronchoscope and airway, while stiffness provides a stable platform for surgical operations, such as biopsies [36]. One benefit of the proposed ES is the ability to alter its rigidity by

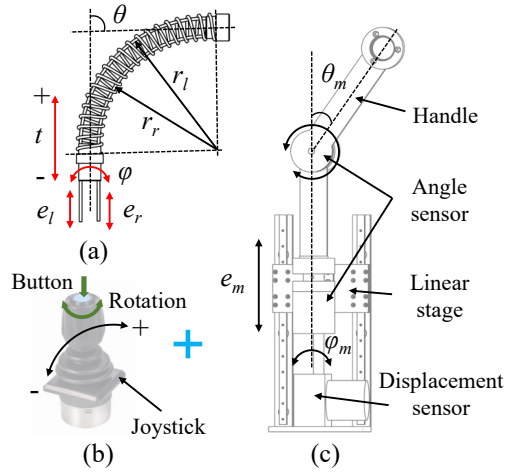

Fig. 5. The mapping relationship between the proposed master device and the slave device of the extensible bronchoscope.

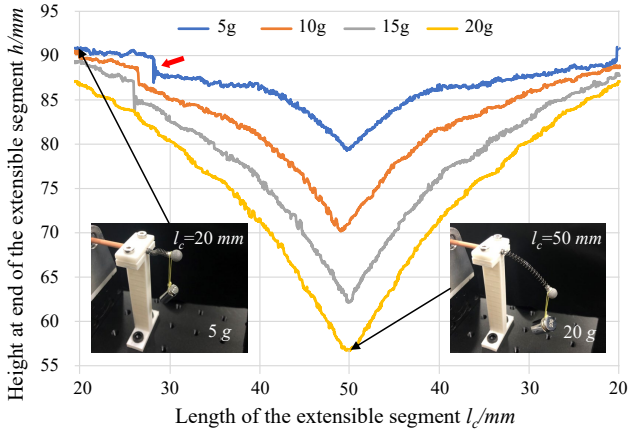

Fig. 6. Stiffness variation of the proposed ES at different bending lengths.

adjusting the bending length whilst sustaining the orientation of the tip of the segment. Refer to [27], the bending stiffness of the ES K_{es} is,

$$K_{es} = 2K_r + K_s = \frac{2E_r G_r \pi {r_{rod}}^4}{(E_r + 2G_r) l_{rod}} + \frac{E_s {d_w}^4}{32nD}\left(\frac{1}{1 + \frac{E_s}{2G_s}}\right). \quad (6)$$

Where the notations are as follows: K_r: bending stiffness of driven rods, K_s: bending stiffness of spring, E_r and E_s: elastic modulus of the Ni-Ti rod and the spring, G_r and G_s: Shear modulus of the Ni-Ti rod and the spring, r_{rod}: radius of the rod, l_{rod}: length of the rod. From (6), it can be observed that reducing l_{rod} will result in an increase in K_{es}. On the other hand, the K_s is not affected by the length l_{rod}.

D. Master-Slave Mapping

Teleoperation, also referred to as master-slave control, is the prevalent method of control in surgical robotics, whether in bronchial robots [8] or endoscope surgery robots [37]. Isomorphic master and slave devices maintain an intuitive control system and subsequently lower the learning burden for surgeons. To intuitively teleoperate the ERB, a custom master device has been developed, as shown in Fig. 5.

The ES possesses four degrees of freedom (DoFs) [Fig. 5(**a**)]: the translation t, the rotation φ, the bending angle θ, and the extension (denoted by e_l and e_r). One by one, the master device also has four DoFs. As shown in Fig. 5(**b**), the joystick can be pushed back and forth, and upon exceeding a specific range, the ERB commences movement at a designated speed. For the other three DoFs (two angle sensors and one displacement sensor), we have,

$$\begin{bmatrix} \theta \\ \varphi \\ e_l \\ e_r \end{bmatrix} = \begin{bmatrix} \gamma_1 & \gamma_2 & \gamma_3 & \gamma_4 \end{bmatrix} \begin{bmatrix} \theta_m \\ \varphi_m \\ e_m \\ e_m \end{bmatrix}. \quad (7)$$

Where, $\gamma_i (i = 1, 2, 3, 4)$ are scale factors which can be set according to the need for intuitive control. Note that if the ERB moves in a fixed angle mode, γ_3 equals γ_4, whereas if the ERB moves in a fixed radius mode, they are proportional and can be derived from (5).

There are two auxiliary DoFs as shown in Fig. 5(**b**). The button is designated to alter the propelling motion modes of the ERB between the fixed-angle mode and fixed-radius mode. The rotation is for selecting the desired control, since there may be ambiguity in extension e_l and e_r when linear stage translation e_m and rotation θ_m alter simultaneously.

V. Experiments

A. Stiffness Experiments

An ES is placed horizontally and end loaded, which is the most challenging situation for stiffness testing. A passive marker is fixed to the end of the ES (see insets in Fig. 6), which can be captured by the optitrack camera (V120: TRIO, NaturalPoint, Inc.). The ES is initially stretched from 20 mm to 50 mm and then contracted back to 20 mm with varying masses (5 g, 10 g, 15 g, and 20 g). The recorded data are displayed in Fig. 6. The stiffness of the segment is characterised by the change in height at the end point of the ES. According to the results, the stiffness increases as the length of the ES decreases. Specifically, when the length is reduced from 50 mm to 20 mm, the stiffness of the ES increases by almost tenfold.

In addition, the data fluctuates slightly and is asymmetrical about the line l_c =50 mm due to friction and return errors of the driven Ni-Ti rods. The issue can be mitigated through motion compensation and optimal structural design for future experiments. When the ES is shortened to a certain extent, the spring will buckle in the direction perpendicular to the plane where the two driven rods are located, forming an S shape (refer to the left inset and the fluctuations in Fig. 6 with the red arrow). Although this does not affect the steering ability of the ES, we will incorporate extra passive rods to restrict the longitudinal movement of the spring in the future.

B. Follow-The-Leader Motion

To validate the FTL performance of the ES, experiments have been carried out and the results are shown in Fig. 7.

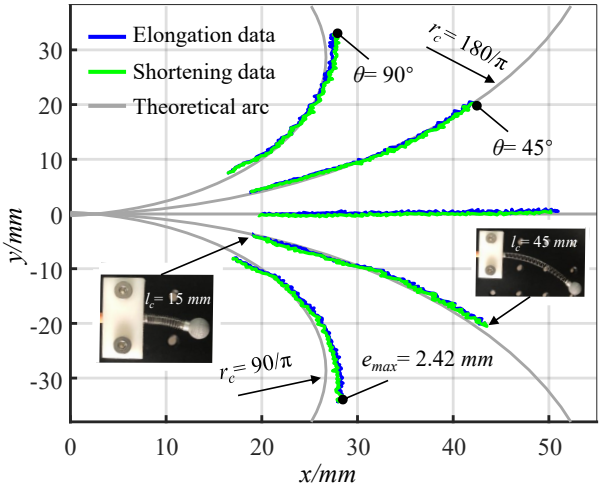

Fig. 7. Experimental results of the proposed ES moving in the follow-the-leader motion mode.

The fixe-angle motion performance can be found in [27].

The experimental setup is analogous to that employed in stiffness experiments. The ES elongates from l_c =15 mm to l_c =45 mm (20 mm to 50 mm for the centre of the passive marker) with three intended bending angles (0°, 45°, 90°). Fig. 7 is theoretically symmetrical up and down. It is clear that the process of segment elongation and shortening is generally uniform, despite some deviations between the actual and ideal results. The largest difference is 2.42 mm when l_c equals 45 mm and θ equals 90°. This could be attributed to the larger bending angle that applies more pressure on the driven rods, resulting in greater deformation and increased error. However, with master-slave operation, this error is still within an acceptable range.

C. Phantom Experiments

An airway model is produced via 3D printing, following the dimension analysis discussed in section II. This model is then utilised in the phantom experiments, with the experimental setup illustrated in Fig. 8 (**a**) and Fig. 8 (**b**). The aim of the experiments is to showcase the benefits of the ERB.

As demonstrated in Fig. 8(**d**), a traditional bronchoscope with a long bending segment might be stuck in narrow corners. On the other hand, if the bronchoscope's bending length is too short, it may result in steering failure [see Fig. 8(**c**)]. By contrast, the ERB offers superior steering capability by adjusting the bending segment length [see Fig. 8(**e**)]. In addition to providing a stable biopsy platform, the stiffness adjustment of the ES can also enhance the steering ability as shown in Fig. 8(**f**) and Fig. 8(**g**). When the push force is transmitted through the flexible tube, the ES may deflect into an undesired shape (known as looping [38]) [see Fig. 8(**f**)] due to its lower stiffness compared to the tube (although the stiffness difference between the two is not our focus, we aim to make them more compatible in future work). In this condition, the shortened segment can improve the bending segment stiffness, aiding in steering, as demonstrated in Fig. 8(**g**). To mitigate the effect of

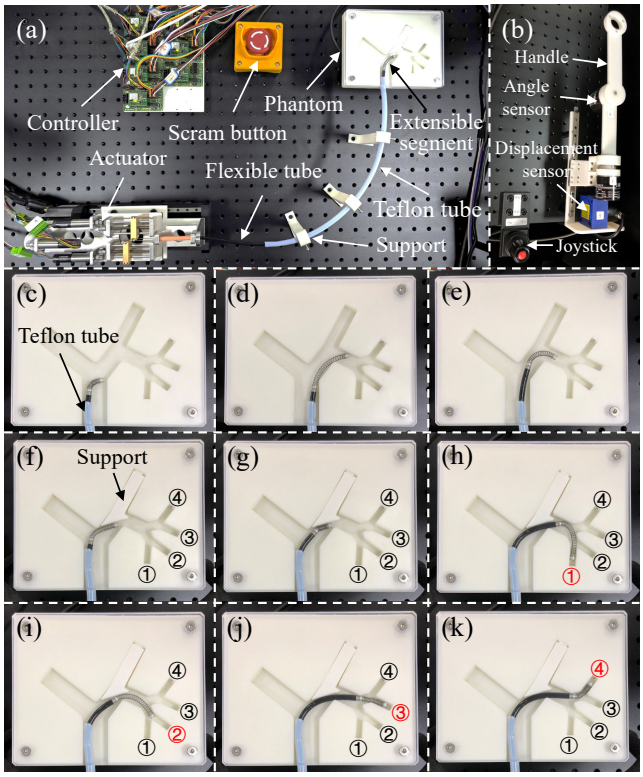

Fig. 8. Experimental setup for phantom experiments including the proposed ERB (**a**) and the master device (**b**), and experimental results (**c**)-(**k**) of the proposed ES steering in an airway phantom.

the greater stiffness of the flexible tube, a small printed support is utilized as illustrated in Fig. 8(**f**). Together with its extensible characteristics, the segment can reach three targets successfully as shown in Fig. 8(**h**), Fig.8(**j**), and Fig.8(**k**). For the second target [see Fig.8(**i**)], the ERB is restricted by the actuator's limited range of motion, requiring further research. Additional details are available in the accompanying video.

VI. Conclusion

In this paper, we propose an extensible robot-assisted bronchoscope comprising a robotic arm, actuator, flexible tube, and extensible segment. The ERB's steering ability is enhanced by adjusting the bending segment length. We thoroughly analyse the workspace i.e., the range of motion, based on forward kinematics, as well as the fixed-angle and the follow-the-leader modes for motion control. An custom master device is developed for intuitive control of the proposed ERB. Phantom experiments in master-slave control mode show the advantages of the extensible bronchoscope and validate the proposed ERB.

In future research, the proposed ERB will incorporate cameras and biopsy forceps, and subsequently be validated in three-dimensional airway models and animal experiments. Additionally, the ERB system will incorporate AI-enhanced medical imaging [39] and navigation technologies [40], in preparation for future clinical applications.

REFERENCES

[1] R. L. Siegel, K. D. Miller, N. S. Wagle, and A. Jemal, "Cancer statistics, 2023," *Ca Cancer J Clin*, vol. 73, no. 1, pp. 17–48, 2023.

[2] J. E. Cox, C. Chiles, C. M. McManus, S. L. Aquino, and R. H. Choplin, "Transthoracic needle aspiration biopsy: variables that affect risk of pneumothorax," *Radiology*, vol. 212, no. 1, pp. 165–168, 1999.

[3] D. G. Nicastri and T. S. Weiser, "Rigid bronchoscopy: indications and techniques," *Operative Techniques in Thoracic and Cardiovascular Surgery*, vol. 17, no. 1, pp. 44–51, 2012.

[4] T. S. Panchabhai and A. C. Mehta, "Historical perspectives of bronchoscopy. connecting the dots," *Annals of the American Thoracic Society*, vol. 12, no. 5, pp. 631–641, 2015.

[5] J. S. W. Memoli, P. J. Nietert, and G. A. Silvestri, "Meta-analysis of guided bronchoscopy for the evaluation of the pulmonary nodule," *Chest*, vol. 142, no. 2, pp. 385–393, 2012.

[6] N. T. Tanner, L. Yarmus, A. Chen, J. W. Memoli, H. J. Mehta, N. J. Pastis, H. Lee, M. A. Jantz, P. J. Nietert, and G. A. Silvestri, "Standard bronchoscopy with fluoroscopy vs thin bronchoscopy and radial endobronchial ultrasound for biopsy of pulmonary lesions: a multicenter, prospective, randomized trial," *Chest*, vol. 154, no. 5, pp. 1035–1043, 2018.

[7] A. Chen, N. Pastis, B. Furukawa, and G. A. Silvestri, "The effect of respiratory motion on pulmonary nodule location during electromagnetic navigation bronchoscopy," *Chest*, vol. 147, no. 5, pp. 1275–1281, 2015.

[8] A. Agrawal, D. K. Hogarth, and S. Murgu, "Robotic bronchoscopy for pulmonary lesions: a review of existing technologies and clinical data," *Journal of thoracic disease*, vol. 12, no. 6, p. 3279, 2020.

[9] A. J. Kent, K. A. Byrnes, and S. H. Chang, "State of the art: robotic bronchoscopy," in *Seminars in Thoracic and Cardiovascular Surgery*, vol. 32, no. 4. Elsevier, 2020, pp. 1030–1035.

[10] S. Choi, E. A. Hoffman, S. E. Wenzel, M. Castro, S. B. Fain, N. N. Jarjour, M. L. Schiebler, K. Chen, and C.-L. Lin, "Quantitative assessment of multiscale structural and functional alterations in asthmatic populations," *Journal of applied physiology*, vol. 118, no. 10, pp. 1286–1298, 2015.

[11] P. E. Dupont, J. Lock, B. Itkowitz, and E. Butler, "Design and control of concentric-tube robots," *IEEE Transactions on Robotics*, vol. 26, no. 2, pp. 209–225, 2009.

[12] J. Wang, X. Yang, P. Li, S. Song, L. Liu, and M. Q.-H. Meng, "Design of a multi-arm concentric-tube robot system for transnasal surgery," *Medical & biological engineering & computing*, vol. 58, pp. 497–508, 2020.

[13] Z. Li, P. W. Chiu, and R. Du, "Design and kinematic modeling of a concentric wire-driven mechanism targeted for minimally invasive surgery," in *2016 IEEE/RSJ International Conference on Intelligent Robots and Systems (IROS)*. IEEE, 2016, pp. 310–316.

[14] A. Degani, H. Choset, A. Wolf, and M. A. Zenati, "Highly articulated robotic probe for minimally invasive surgery," in *Proceedings 2006 IEEE International Conference on Robotics and Automation, 2006. ICRA 2006.* IEEE, 2006, pp. 4167–4172.

[15] E. Amanov, J. Granna, and J. Burgner-Kahrs, "Toward improving path following motion: hybrid continuum robot design," in *2017 IEEE international conference on robotics and automation (ICRA)*. IEEE, 2017, pp. 4666–4672.

[16] X. Duan, D. Xie, R. Zhang, X. Li, J. Sun, C. Qian, X. Song, and C. Li, "A novel robotic bronchoscope system for navigation and biopsy of pulmonary lesions," *Cyborg and Bionic Systems*, vol. 4, p. 0013, 2023.

[17] X. Zhang, W. Li, P. W. Y. Chiu, and Z. Li, "A novel flexible robotic endoscope with constrained tendon-driven continuum mechanism," *IEEE Robotics and Automation Letters*, vol. 5, no. 2, pp. 1366–1372, 2020.

[18] Z. Li, H. Yu, H. Ren, P. W. Chiu, and R. Du, "A novel constrained tendon-driven serpentine manipulator," in *2015 IEEE/RSJ International Conference on Intelligent Robots and Systems (IROS)*. IEEE, 2015, pp. 5966–5971.

[19] J. Chen, Q. Ding, W. Yan, K. Yan, J. Chen, J. Y.-K. Chan, and S. S. Cheng, "A variable length, variable stiffness flexible instrument for transoral robotic surgery," *IEEE Robotics and Automation Letters*, vol. 7, no. 2, pp. 3835–3842, 2022.

[20] C. Culmone, S. F. Yikilmaz, F. Trauzettel, and P. Breedveld, "Follow-the-leader mechanisms in medical devices: A review on scientific and patent literature," *IEEE Reviews in Biomedical Engineering*, 2021.

[21] E. Amanov, T.-D. Nguyen, and J. Burgner-Kahrs, "Tendon-driven continuum robots with extensible sections—a model-based evaluation of path-following motions," *The International Journal of Robotics Research*, vol. 40, no. 1, pp. 7–23, 2021.

[22] T.-D. Nguyen and J. Burgner-Kahrs, "A tendon-driven continuum robot with extensible sections," in *2015 IEEE/RSJ International Conference on Intelligent Robots and Systems (IROS)*. IEEE, 2015, pp. 2130–2135.

[23] B. Kang, R. Kojcev, and E. Sinibaldi, "The first interlaced continuum robot, devised to intrinsically follow the leader," *PloS one*, vol. 11, no. 2, p. e0150278, 2016.

[24] P. W. Henselmans, S. Gottenbos, G. Smit, and P. Breedveld, "The memo slide: An explorative study into a novel mechanical follow-the-leader mechanism," *Proceedings of the Institution of Mechanical Engineers, Part H: Journal of Engineering in Medicine*, vol. 231, no. 12, pp. 1213–1223, 2017.

[25] C. Culmone, D. J. Jager, and P. Breedveld, "Memobox: A mechanical follow-the-leader system for minimally invasive surgery," *Frontiers in Medical Technology*, vol. 4, p. 938643, 2022.

[26] J. Wang, C. Hu, G. Ning, L. Ma, X. Zhang, and H. Liao, "A novel miniature spring-based continuum manipulator for minimally invasive surgery: Design and evaluation," *IEEE/ASME Transactions on Mechatronics*, 2023.

[27] J. Wang, C. Hu, Y. Sun, L. Ma, G. Ning, and H. Liao, "Preliminary study of a spring-based miniature extensible manipulator for bronchoscopic steering," in *2023 IEEE International Conference on Robotics and Biomimetics (ROBIO)*. IEEE, 2023, pp. 1–6.

[28] M. Zhang, Y. Wu, H. Zhang, Y. Qin, H. Zheng, W. Tang, C. Arnold, C. Pei, P. Yu, Y. Nan, *et al.*, "Multi-site, multi-domain airway tree modeling (atm'22): A public benchmark for pulmonary airway segmentation," *arXiv preprint arXiv:2303.05745*, 2023.

[29] D. E. Ost, A. Ernst, X. Lei, K. L. Kovitz, S. Benzaquen, J. Diaz-Mendoza, S. Greenhill, J. Toth, D. Feller-Kopman, J. Puchalski, *et al.*, "Diagnostic yield and complications of bronchoscopy for peripheral lung lesions. results of the aquire registry," *American journal of respiratory and critical care medicine*, vol. 193, no. 1, pp. 68–77, 2016.

[30] S. I. Odronic, T. R. Gildea, and D. J. Chute, "Electromagnetic navigation bronchoscopy-guided fine needle aspiration for the diagnosis of lung lesions," *Diagnostic cytopathology*, vol. 42, no. 12, pp. 1045–1050, 2014.

[31] L. Dupourqué, F. Masaki, Y. L. Colson, T. Kato, and N. Hata, "Transbronchial biopsy catheter enhanced by a multisection continuum robot with follow-the-leader motion," *International journal of computer assisted radiology and surgery*, vol. 14, no. 11, pp. 2021–2029, 2019.

[32] M. Montaudon, P. Desbarats, P. Berger, G. De Dietrich, R. Marthan, and F. Laurent, "Assessment of bronchial wall thickness and lumen diameter in human adults using multi-detector computed tomography: comparison with theoretical models," *Journal of anatomy*, vol. 211, no. 5, pp. 579–588, 2007.

[33] S. Takase, "Flexible endoscope," June 3 2003, uS Patent 6,572,538.

[34] Y. Zou, B. Guan, J. Zhao, S. Wang, X. Sun, and J. Li, "Robotic-assisted automatic orientation and insertion for bronchoscopy based on image guidance," *IEEE Transactions on Medical Robotics and Bionics*, vol. 4, no. 3, pp. 588–598, 2022.

[35] A. Wahl and K. Bisshopp, "Mechanical springs," *Journal of Applied Mechanics*, vol. 31, no. 1, p. 159, 1964.

[36] D. Van Lewen, T. Janke, H. Lee, R. Austin, E. Billatos, and S. Russo, "A fluidic actuated soft robot for improving bronchoscopic biopsy," in *2023 Hamlyn Symposium on Medical Robotics*, 2023.

[37] B. S. Peters, P. R. Armijo, C. Krause, S. A. Choudhury, and D. Oleynikov, "Review of emerging surgical robotic technology," *Surgical endoscopy*, vol. 32, pp. 1636–1655, 2018.

[38] A. Loeve, P. Breedveld, and J. Dankelman, "Scopes too flexible... and too stiff," *IEEE pulse*, vol. 1, no. 3, pp. 26–41, 2010.

[39] Y. Sun, Q. Yao, Y. Lyu, J. Wang, Y. Xiao, H. Liao, and S. K. Zhou, "Rib suppression in digital chest tomosynthesis," in *International Conference on Medical Image Computing and Computer-Assisted Intervention*. Springer, 2022, pp. 696–706.

[40] L. Ma, T. Huang, J. Wang, and H. Liao, "Visualization, registration and tracking techniques for augmented reality guided surgery: a review," *Physics in Medicine & Biology*, 2022.